A concave photonic crystal waveguide with a corrugated surface for high-quality focusing

Hong Wu (武 红)[1], Liyong Jiang (蒋立勇)[1*], Haipeng Li (李海鹏)[2], Wei Jia (贾 巍)[1], Gaige Zheng (郑改革)[3], Haixia Qiang (强海霞)[1], and Xiangyin Li (李相银)[1]**

[1]*Department of Physics, Nanjing University of Science and Technology, Nanjing 210094, China*

[2]*Nanoscale Technology and Engineering Laboratory, Department of Mechanical Engineering, Schulich School of Engineering, University of Calgary, Calgary, Alberta, T2N 2N4, Canada*

[3]*Tanaka Metamaterials Laboratory, RIKEN, Saitama 351-0198, Japan*

[*]*Corresponding author: jly@mail.njust.edu.cn;* [**]*corresponding author: xyl@mail.njust.edu.cn*

Received June 8, 2010; accepted September 10, 2010; posted online January 1, 2011

A concave two-dimensional (2D) photonic crystal waveguide (PCW) with corrugated surface is theoretically used as a focusing structure. To design this structure, a genetic algorithm is combined with the finite-difference time-domain method. For PCWs with different degrees of concaveness, the power reaches about 80% at different focusing points when the morphology of the concave surface is optimized. More importantly, the focusing location is easily controlled by changing the location of the detector placed in the output field.

OCIS codes: 130.5296, 130.3120.
doi: 10.3788/COL201109.011301.

Photonic crystal waveguide (PCW)[1,2], created by introducing line defects in the bulk crystal, is one of the key components of integrated optical devices because it forms a medium for light path propagation in photonic integrated circuits[3]. However, one of the problems preventing the wider commercial application of photonic crystals (PCs) is the difficulty in coupling PCWs with other devices, such as optical fibers. A possible solution involves tapering the waveguide to achieve better coupling with the fiber[4−6]. Recently, many researchers have managed to manipulate the dispersed light at the outlet of a PCW. In these studies, modifying the termination of the PCW with planar surface corrugation has been demonstrated as a simple and efficient way to freely control the electric field distribution of the excited waves to yield directional emission beams[7−9], splitting beams[10], and focusing effects[11]. These effects are due to the interference of light emitted from leaky surface modes along the surface corrugation[12].

In this letter, we focus on the design of the corrugated surface for constructing a high-quality focusing system. The corrugated surface and the PCW used in this study are assumed as concave, which has been demonstrated more effective than conventional planar types[11,13]. To design such complex structures, in contrast to previous studies, a global optimization method is adopted, which has been shown superior in designing planar corrugated surface for producing high-quality directional emissions[14] and splitting beam effects[10]. Based on similar mechanisms, considerable enhancement of the quality of the focusing point is expected in terms of focusing power, full-width at half-maximum (FWHM), and focal length if global optimization is implemented for the concave corrugated surface.

As indicated in Fig. 1(a), the proposed model is formed by a concave two-dimensional (2D) PC structure with radius R. The pillar-type PC structure[15] consists of a square array of Si dielectric rods with refractive index of 3.45. The radii of the rods are r=0.2a (where a is the lattice constant of bulk PC). For transverse-electric (TE) polarization, i.e., electric field oriented along the rod axis, the photonic band gap (PBG) of the PC structure is calculated through the plane wave expansion (PWE) method[16] and can be presented in a normalized frequency range of (0.278–0.424)×(2πc/a)[13], where c is the light velocity in vacuum. A row of rods along the z-direction is removed from the 2D PC mentioned above to form a 2D PCW. The size of the waveguide is 23a in the x-direction and 10a in the z-direction. Due to the symmetry of the system, the concave corrugated surface is divided into two symmetrical subsurfaces along the axis x=0. As shown in Fig. 1(b), the surface is described by six parameters: x_1, x_2, x_3, x_4, x_5, and x_6. Here, x_1 and x_2 represent the diameters of the odd rods and the even rods along the surface, respectively; x_3 represents the lattice period of the surface rods; x_4 is the distance of each subsurface from axis x=0; x_5 and x_6 represent the distances of the odd rods and the even rods to the termination of the PCW, respectively.

For the concave structure, a power detector with cross-sectional width l is placed at a specific location (x_D, z_D) in the output field to characterize the transmission of light emitted from the PCW (Fig. 1(a))[8]. The normalized detector power $P_D(\omega_0)$, obtained as a time average by finite-difference time-domain (FDTD) method, can be expressed by the equations in Ref. [14]. The genetic algorithm (GA) is used to provide global designs for such concave structures by searching the maximum value of $P_D(\omega_0)$. As a representation of the new generation of global optimization algorithms, GA is quite different from many local optimization methods and other traditional global optimization methods. Many previous studies have also proven its clear advantage in designing complicated PC devices[17,18]. Hence, GA is very

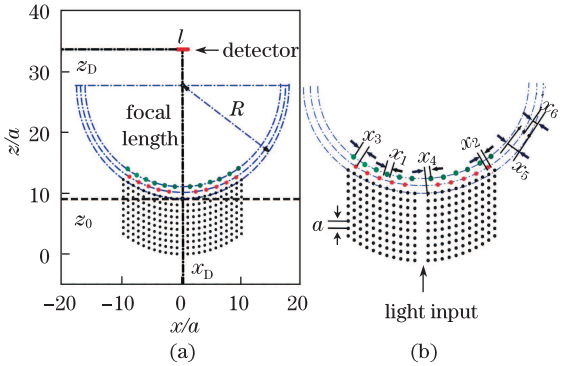

Fig. 1. (a) Schematic diagram of the PC structure for optimization; (b) parameters of the concave corrugated surface for optimization.

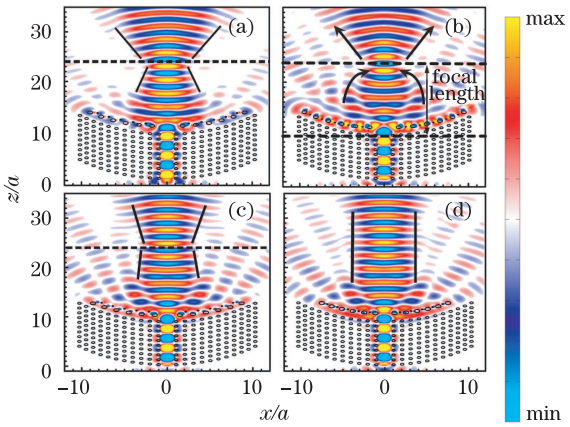

Fig. 2. Electric-field amplitude distributions for (a) Project 1, (b) Project 2, (c) Project 3, and (d) Project 4.

suitable to deal with the optimization of the corrugated surface proposed in our study by combining it with the FDTD. Details of the combined technique are available in Ref. [14].

Based on our experience, the detector cross-sectional width l is an important factor that influences the final focusing effect. Hence, choosing an appropriate value of l is necessary for obtaining high-quality designs. In previous reports, the FWHM at the focusing point generally ranged from $1a$ to $4a$. Thus, we first tried four GA projects considering different l: Project 1, l=$1a$; Project 2, l=$2a$; Project 3, l=$3a$; and Project 4, l=$4a$. In these projects, the frequency of the Gaussian continuous wave was set to $0.368(2\pi c/a)$ and the radius of the concave curvature was set to $15a$. The detector in each project was placed at the same point ($x_{\rm D}$=0, $z_{\rm D}$=$24a$). The final optimal corrugated surfaces of each project are represented as follows: (Project 1) x_1=$0.58a$, x_2=$0.20a$, x_3=$0.90a$, x_4=$0.88a$, x_5=$1.68a$, and x_6=$1.99a$; (Project 2) x_1=$0.58a$, x_2=$0.14a$, x_3=$0.96a$, x_4=$0.83a$, x_5=$1.68a$, and x_6=$1.69a$; (Project 3) x_1=$0.60a$, x_2=$0.18a$, x_3=$0.83a$, x_4=$0.49a$, x_5=$1.37a$, and x_6=$1.98a$; (Project 4) x_1=$0.64a$, x_2=$0.20a$, x_3=$0.78a$, x_4=$0.21a$, x_5=$1.66a$, and x_6=$1.81a$.

To verify the focusing effect of these structures directly, the electric-field amplitude distribution was calculated, as indicated in Fig. 2. When l was set to $1a$ and $2a$, a clear focusing effect was observed in both Figs. 2(a) and (b). The focusing point emerged at around $x_{\rm D}$=0, $z_{\rm D}$=$24a$, which is in good agreement with the predefined location of the detector. As l was increased to $3a$, the focusing effect became unclear (Fig. 2(c)) and even degenerated to a nice beaming effect (Fig. 2(d)) when it reached $4a$. The normalized power transmission at the focusing location is plotted in Fig. 3(a). When l was increased from $1a$ to $4a$, the FWHM did not monotonously increase, instead it reached its minimum at $2.6a$ when l was $2a$. The power transmissions at the focusing location for the four projects were 86.3%, 81.3%, 84.2%, and 83.2%, respectively. Considering both the focusing power and FWHM, the detector width was set to $2a$ in the design of the high-quality focusing structures in subsequent projects. Furthermore, when the detector in each project was placed at the same point, the focal point for each optimized structure was located at approximately the detector location (except for Project 4). This indicates that controlling the focusing position is possible by changing the detector location.

In Ref. [13], the authors found that if the concave curvature increases, the focusing point moves farther from the termination of the PCW, and this phenomenon was explained using the Rowland grating theory. However, they did not mentioned whether high focusing can also be maintained when only the concave curvature is changed. This means that designing a high-quality focusing system with any predefined focal length is still a challenge. In the following projects, we tried to solve this problem. The subsequent experiments were performed using the same surface parameters as in Project 2 with varying radius R. Figures 4(a) and (b) show the electric-field amplitude distribution when R was $20a$ and $25a$, respectively. When R was increased from $20a$ to $25a$, the focal length increased from $18a$ to $22a$, but the focusing power decreased from 70.8% to 66.5%. Hence, high focusing cannot be maintained if only the concave curvature of the PCW is changed. To improve the quality of focusing systems in Figs. 4(a) and (b), two GA projects were executed. For Project 5, the radius R was $20a$ and the detector location was ($x_{\rm D}$=0, $z_{\rm D}$=$27a$), whereas for Project 6, the radius R was $25a$ and the detector location was ($x_{\rm D}$=0, $z_{\rm D}$=$31a$). The final optimal designs are represented as follows: (Project 5) x_1=$0.22a$, x_2=$0.60a$, x_3=$0.79a$, x_4=$0.09a$, x_5=$1.57a$, and x_6=$1.63a$; and (Project 6) x_1=$0.58a$, x_2=$0.18a$, x_3=$0.77a$, x_4=$0.84a$, x_5=$1.55a$, and x_6=$1.99a$. Figures 4(c) and (d) illustrate the corresponding electric-field amplitude distributions for Projects 5 and 6, respectively. As expected, the light beams were focused at the predefined location and the focusing power reached 80.5% and 86.7%, respectively. The normalized power transmissions at the focusing location are plotted in Fig. 3(b). Compared with the unoptimized structures in Figs. 4(a) and (b), the FWHMs of the optimized structures in Figs. 4(c) and (d) are all reduced. Based on this phenomenon, our combined design method can conclusively be used to produce high-quality focusing systems with arbitrary focal lengths as needed.

The focusing power in Projects 2, 5, and 6 were much higher (more than 80%) than those reported in Ref. [11] (less than 30%). Consequently, we tried to account for this through physical mechanisms. As demonstrated by many previous studies, GA is an effective global

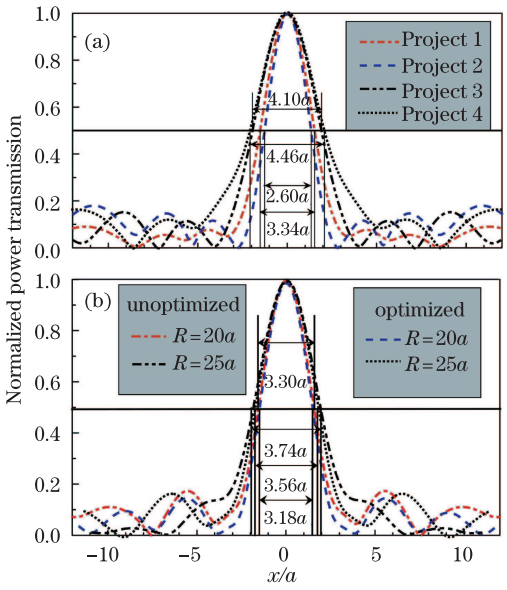

Fig. 3. Normalized power transmission at the focusing locations for different structures: (a) Projects 1–4 and (b) unoptimized and optimized structures with different degrees of concaveness.

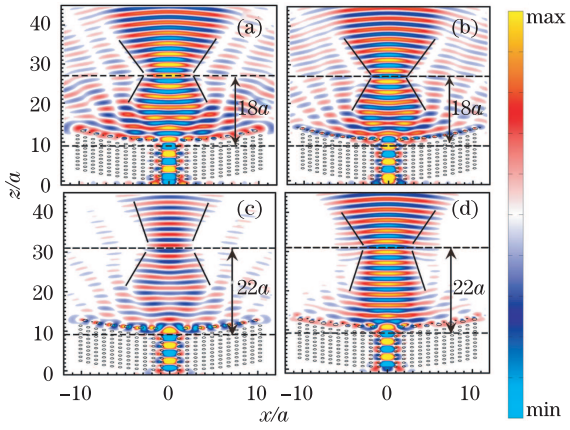

Fig. 4. Electric-field amplitude distributions for PCWs with different degrees of concaveness: (a) unoptimized structure with R=20a; (b) unoptimized structure with R=25a; (c) Project 5, optimized structure with R=20a; and (d) Project 6, optimized structure with R=25a.

optimization method for dealing with complex problems in which the physical details are relatively unclear. For our proposed model, the focusing effect is mainly due to the interference of surface modes excited by the waves from the outlet of the PCW and influenced by the coupling efficiency between the output waves and the surface modes. Unfortunately, at present, to our knowledge, no concrete formulation has been reported to exactly describe the relationship of the surface parameters with the coupling efficiency, as well as the interference effect of the surface modes. Providing such a formulation was avoided in this letter. Instead, the maximum power of the detector was directly determined to automatically optimize the coupling efficiency and other factors to construct a high-quality focusing point. This is an inverse strategy to solve such a problem.

In addition, the corrugated surface and the whole PCW optimized in this letter were assumed as concave. For

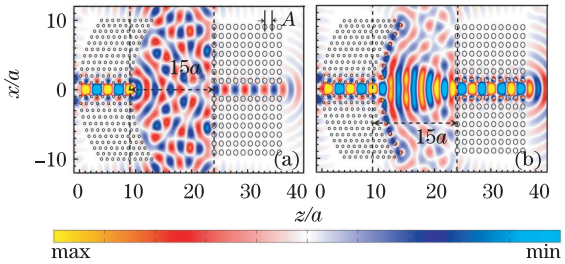

Fig. 5. Electric-field amplitude distributions for coupling between a straight standard PCW and a concave PCW (a) without corrugated surface and (b) with the optimum corrugated surface.

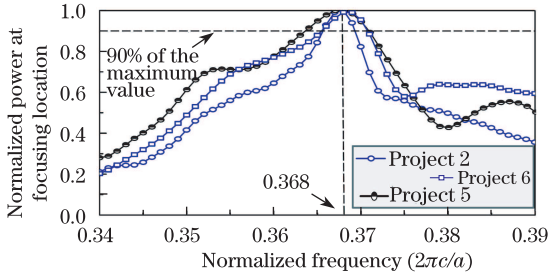

Fig. 6. Normalized power at the focusing location versus wavelength for the optimal structure in Projects 2, 5, and 6.

far-field imaging, a similar concave structure has been proposed in PC concave lenses[19] using negative refraction, which reduces aberration for the same radius of curvature. However, our proposed focusing structures are intended as the output coupler for photonic integrated circuits comprising PCWs. Hence, taking the optimal design in Project 2 as an example, a check was performed to determine how the proposed focusing structure integrated with standard straight PCWs. As shown in Fig. 5, the right straight PCW is formed by removing a row of rods along the z-direction from a square lattice PC. The radii of the rods are r=0.3A, where A is the lattice constant of the bulk PC. For TE polarization, the PBG normalized frequency of the PC structure ranged between (0.410–0.511)×($2\pi c/A$). To reduce the coupling less induced by the difference between the width of the light beam and the width of the right straight PCW, the lattice constant A was set to 1.3a because the FWHM at the focusing location in Project 2 was 2.6a. As a result, the frequency of the input Gaussian wave was 0.368($2\pi c/a$), which corresponds to the guiding frequency (0.478($2\pi c/A$)) of the straight PCW. The inlet of the straight PCW was placed at point ($x_{\rm D}$=0, $z_{\rm D}$=24a) so that the coupling length was 15a, the focal length of the focusing system. For the coupling between a non-corrugated concave PCW and the straight PCW, Fig. 5(a) presents the corresponding electric-field amplitude distribution. The light energy from the left waveguide underwent a rapid angle divergence due to diffraction, with only 20.7% of the energy coupled to the right waveguide and most of the energy was wasted. When the optimal corrugated surface was added behind the concave PCW, as indicated in Fig. 5(b), the power forms a focal point at approximately 24a, and 97% of the focusing energy was coupled to the right waveguide. This indicates that high-quality focusing structures can be used as couplers for connecting PCWs to conventional

PCWs and even optical fibers.

As shown in Fig. 6, the relationship between detector power and frequency for Projects 2, 5, and 6 indicates a maximum focusing power of $0.368(2\pi c/a)$ for the three projects. If a working frequency band was defined by assuming that the power is higher than 90% of the maximum value, the working frequency band is accepted within the ranges $[0.366(2\pi c/a), 0.369(2\pi c/a)]$, $[0.364(2\pi c/a), 0.370(2\pi c/a)]$, and $[0.366(2\pi c/a), 0.370(2\pi c/a)]$ for the three structures, respectively.

In conclusion, to enhance the focusing quality of a PCW with a concave corrugated surface, the surface parameters of the corrugated surface have been globally optimized using a combination of GA and FDTD. The optimization results indicate that high-quality focusing systems can be obtained if the cross-sectional width of the detector is set to an appropriate value. For PCWs with varying concaveness, high-quality focusing systems can be designed with different focal lengths by optimizing the surface structures. These effective focusing designs have some potential applications for connecting integrated optical devices.

This work was supported by research funding from the Nanjing University of Science and Technology (Nos. 2010ZYTS059 and AE88030) and the Natural Science Foundation of Jiangsu Province (No. BK2010483).

References

1. S. G. Johnson, P. R. Villeneuve, S. Fan, and J. D. Joannopoulos, Phys. Rev. B **62,** 8212 (2000).
2. E. H. Khoo, T. H. Cheng, A. Q. Liu, J. Li, and D. Pinjala, Appl. Phys. Lett. **91,** 171109 (2007).
3. S. H. G. Teo, A. Q. Liu, J. B. Zhang, and M. H. Hong, Appl. Phys. Lett. **89,** 091910 (2006).
4. E. H. Khoo, A. Q. Liu, J. H. Wu, J. Li, and D. Pinjala, Opt. Express **14,** 6035 (2006).
5. E. H. Khoo, A. Q. Liu, X. M. Zhang, E. P. Li, J. Li, D. Pinjala, and B. S. Luk'yanchuk, Phys. Rev. B **80,** 035101 (2009).
6. S. Chen, G. Zhu, T. Yu, Q. Liao, N. Liu, and Y. Huang, Acta Opt. Sin. (in Chinese) **29,** 2898 (2009).
7. E. Moreno, F. J. García-Vidal, and L. Martín-Moreno, Phys. Rev. B **69,** 121402(R) (2004).
8. S. K. Morrison and Y. S. Kivshar, Appl. Phys. Lett. **86,** 081110 (2005).
9. K. B. Chung, Opt. Commun. **281,** 5349 (2008).
10. L. Jiang, W. Jia, H. Li, X. Li, C. Cong, and Z. Shen, J. Opt. Soc. Am. B **26,** 2157 (2009).
11. H. Chen, Y. Zeng, X. Chen, J. Wang, and W. Lu, Phys. Lett. A **372,** 5096 (2008).
12. W. Śmigaj, Phys. Rev. B **75,** 205430 (2007).
13. E. H. Khoo, A. Q. Liu, T. H. Cheng, J. Li, and D. Pinjala, Appl. Phys. Lett. **91,** 221105 (2007).
14. L. Jiang, H. Li, W. Jia, X. Li, and Z. Shen, Opt. Express **17,** 10126 (2009).
15. S. H. G. Teo, A. Q. Liu, J. Singh, and M. B. Yu, J. Vac. Sci. Technol. B **22,** 2640 (2004).
16. M. Zhang, W. Pan, L. Yan, B. Luo, D. Zheng, X. Xu, L. Wang, C. Liu, and H. Liu, Chinese J. Lasers (in Chinese) **36,** 857 (2009).
17. J. Smajic, C. Hafner, and D. Erni, J. Opt. Soc. Am. A **21,** 2223 (2004).
18. L. Sanchis, A. Håkansson, D. López-Zanón, J. Bravo-Abad, and J. Sánchez-Dehesa, Appl. Phys. Lett. **84,** 4460 (2004).
19. P. Vodo, P. V. Parimi, W. T. Lu, and S. Sridhar, Appl. Phys. Lett. **86,** 201108 (2005).